Supplemental Material for:

"Mixture Rules and Falloff are Now Major Uncertainties in Experimentally Derived Rate Parameters for H + O_2 (+M) $\leftrightarrow$ HO_2 (+M)"

Lei Lei[1], **Michael P. Burke**[1,2,*]

[1]*Department of Mechanical Engineering, Columbia University, New York, NY 10027, USA*
[2]*Department of Chemical Engineering, Data Science Institute, Columbia University, New York, NY 10027, USA*

* **Corresponding author information:**

Michael P. Burke
220 S.W. Mudd Building, MC 4703
500 West 120th Street
New York, NY 10027
Email: mpburke@columbia.edu
Phone: +1(212) 851-0782

S1 Dipole-Dipole Capture Rate Constants for HO_2 + H_2O

The dipole-dipole capture rate constants, Z_{d-d}, for HO_2+H_2O at various temperatures, are calculated according to Eq. (16) in [5],

$$Z_{d-d} = f_{rigid}\Gamma(1/3)(\mu_{D_1}\mu_{D_2})^{2/3}(k_BT)^{-1/6}(8\pi/\mu)^{1/2} \tag{S1}$$

where μ_{D_1} and μ_{D_2} are respectively the dipole moments for HO_2 and H_2O here; k_B is the Boltzmann constant; T is the temperature (K); μ is the reduced mass of the system; and the rigidity factor f_{rigid} is obtained from Eq. (2.21) in [9] as $f_{rigid} = k_{cap}/k_{cap}^{PST}$, where the thermal capture rate constants, k_{cap}, and the thermal capture rate constants from phase space theory (PST), k_{cap}^{PST}, are respectively obtained from Eqs. (2.13) and (2.24) in [9], which, for nonidentical dipoles, yields

$$\begin{aligned} f_{rigid} = \frac{k_{cap}}{k_{cap}^{PST}} &= \frac{f(\mu_{D_1}\mu_{D_2})^{1/3}C_6^{1/6}\sqrt{8\pi/\mu}\kappa(\theta,M)}{f\Gamma(1/3)(\mu_{D_1}\mu_{D_2})^{2/3}(k_BT)^{-1/6}\sqrt{8\pi/\mu}} \\ &= \frac{C_6^{1/6}\kappa(\theta,M)}{\Gamma(1/3)(\mu_{D_1}\mu_{D_2})^{1/3}(k_BT)^{-1/6}} \end{aligned} \tag{S2}$$

Thus, Eq.(S1) is further simplified as

$$Z_{d-d} = C_6^{1/6}\kappa(\theta,M)(\mu_{D_1}\mu_{D_2})^{1/3}\sqrt{8\pi/\mu} \tag{S3}$$

where C_6 is the constant of a $-C_6/r^6$ isotropic dispersion potential [9]; and $\kappa(\theta, M)$ is a dimensionless fitting function whose analytical from is reported in Fig. 2 of [9] as a function of the reduced dispersion constant $\theta = C_6k_BT/(\mu_{D_1}\mu_{D_2})^2$ and dimensionless quantity describing degree of adiabaticity, M (not to be confused with the bath gas M).

Table S1: Molecular Parameters Used in the Current Calculations

	HO_2	H_2O	HO_2-H_2O[†]
μ (g/mol)	33.006	18.015	11.654
ϵ/k_B (K)	365.56	535.21	442.32
σ (10^{-10}m)	3.433	2.673	3.053
μ_D (Debye)	2.090	1.847	
B_x (cm^{-1})	20.357	27.877	
B_y (cm^{-1})	1.118	14.512	
B_z (cm^{-1})	1.056	9.285	
B_{tot} (cm^{-1})	0.767	7.530	

[†] ϵ and σ for nonidentical molecule pair HO_2-H_2O are calculated from combination rules

Following [5], the optimized Lennard-Jones parameters and dipole moments from [11] are used for identical particle interactions (i.e. HO_2-HO_2 and H_2O-H_2O, see Table S1), from which the Lennard-Jones parameters for intermolecular dispersion potential between HO_2 and H_2O are estimated using Lorentz-Berthelot rules as $\epsilon_{12} = \sqrt{\epsilon_{11}\epsilon_{22}}$ and $\sigma_{12} = (\sigma_{11} + \sigma_{22})/2$. C_6 is therefore estimated from the Lennard-Jones parameters as $C_6 = 4\epsilon_{12}\sigma_{12}^6$ [5]. To get $\kappa(\theta, M)$, the dimensionless quantity M is first calculated from [9]

$$M = \frac{\mu(\mu_{D_1}\mu_{D_2})^{2/3}(B_1 + B_2)/2}{\hbar^2(k_BT)^{2/3}} \tag{S4}$$

where B_i are the rotational constants for i^{th} particle in the system. Given that both involved particles are polyatomic with three distinct moments of inertia associated with x, y, z directions (Table S1), the rotational constant associated with the direction of dipole moments should be applied. However, if one simply calculates M using the total rotational constants (which are smaller than the appropriate rotational constant), then one could arrive at a lower limit for M (which turns out to be high enough for $\kappa(\theta, M)$ to be independent of M anyway for the present calculations).

Therefore, the results presented here should be relatively insensitive to the choice of rotational constants used in Eq.(S4). Using NIST's Computational Chemistry Comparison and Benchmark DataBase (CCCBDB) [13] for molecular weights and directional rotational constants of HO_2 and H_2O, M is calculated from Eq. (S4). Together with $\theta = C_6 k_B T/(\mu_{D_1}\mu_{D_2})^2$, the values of $\kappa(\theta, M)$ for a specific temperature are read from Fig. 2 of [9] (it can be equivalently calculated using Eqs. (2.14, 2.15, 2.20) in [9] with the parameters from Table I and II in [9]). The dipole-dipole capture rate constants Z_{d-d} are then calculated via Eq. (S3) and tabulated in Table S2 for temperatures of relevant to the current study. (Note that the values in Table S2 differ from those in [5] by up to 25% using apparently the same procedures, though recalculations by [14] yielded the same results as reported here.)

Table S2: Calculated Dipole-Dipole Capture Rate Constants for HO_2 + H_2O at Various Temperatures.

T (K)	$Z_{\text{d-d}}$ (10^{-10} cm^3 molecule^{-1} s^{-1})
200	7.18
300	7.37
400	7.55
500	7.73
600	7.89
700	8.03
800	8.17
900	8.29
1000	8.41
1100	8.52
1200	8.62
1300	8.72
1400	8.81
1500	8.90
1600	8.98
1700	9.06
1800	9.14
1900	9.22
2000	9.29

S2 Deriving Exponential-Down Factors to be Consistent with Reported Experimental Data

Alternative versions of Tables 1 and 2 (which display the $\langle \Delta E_{d,i} \rangle$ values in the 1D-ME model yielding consistency with the reported data) in the main text are provided as Tables S3 and S4 across the full range of experimental pressures (instead of the single representative pressure shown in Tables 1 and 2 used to fit $\langle \Delta E_d \rangle$). These are provided to show the the variation of the extent of falloff of the mixture, $k_{\text{0-eff}}(T, P, \underline{X})/k_0(T, \underline{X})$, across the experimental ranges of pressure (which, as mentioned in the main text, is sufficiently small relative to experimental precision to evade detection).

Equivalent versions of these two tables are presented for the 2D/φ-ME model as Tables S5 and S6. As mentioned in the main text, the exponential-down factors are instead chosen such that the calculated $k_{i,\text{0-eff}}(T, P)$ match the reported $k_{i,\text{0-eff,LMR-P,exp}}(T, P, \underline{X})$ from the experiments (i.e. assuming experiments were conducted in only pure mixtures) – due to the lack of functionality to handle bath gas mixtures in Variflex, the code which implements the 2D/φ-ME model. These tables indicate that the strong-collision limit rate constant from the 2D/φ-ME model using the dipole-dipole collision frequency for HO_2-H_2O are $\sim$30% to a factor of $\sim$3 lower than the experimentally reported rate constants. The $\langle \Delta E_{d,i} \rangle$ parameters derived for the 2D/φ-ME to match experimental data are provided in Table S7.

Table S3: 1D-ME Results at 296 K

M	P (Torr)	$k_{\text{i,0-eff,LMR-P,exp}}(T, P, \underline{X})^{\top}$	$k_{\text{i,0-eff,LMR-P}}(T, P, \underline{X})^{\perp}$	$k_{\text{0-eff}}(T, P, \underline{X})/k_0(T, \underline{X})$	$\langle \Delta E_d \rangle(T)$ †
O_2	25		3.20	0.99	
	50		3.17	0.98	
	75		3.13	0.96	
	100	3.1	3.10	0.95	35.03
	150		3.04	0.94	
	200		2.99	0.92	
Ar/O_2 ‡	25		2.26	0.99	
	50		2.24	0.98	
	75		2.22	0.97	
	100	2.2	2.20	0.96	30.71
	150		2.17	0.95	
	200		2.15	0.94	
N_2/O_2 ‡	25		4.48	0.98	
	50		4.41	0.97	
	75		4.36	0.96	
	100	4.3	4.30	0.94	40.13
	150		4.21	0.92	
	200		4.13	0.91	
H_2O/O_2 ‡	2.2		50.28	1.00	
	2.5		50.17	1.00	
	3		50.04	1.00	
	4		49.93	1.00	
	5	50	49.69	1.00	101.77
	6		49.52	0.99	
	7		49.43	0.99	

$^{\top}$ from [10], units: $10^{-32}\text{cm}^6\text{molecule}^{-2}\text{s}^{-1}$;
$^{\perp}$ calculated using PAPR-MESS, units: $10^{-32}\text{cm}^6\text{molecule}^{-2}\text{s}^{-1}$;
‡ $X_i/X_{O_2} = 98.5\%/1.5\%$ for i = Ar, N_2; $X_i/X_{O_2} = 10\%/90\%$ for $i = H_2O$;
† the listed exponential-down factors in i/O_2 mixtures are for i, units: cm^{-1}.

Table S4: 1D-ME Results at 1200 K

M	P (atm)	$k_{\text{i,0-eff,LMR-P,exp}}(T,P,\underline{X})^{\top}$	$k_{\text{i,0-eff,LMR-P}}(T,P,\underline{X})^{\perp}$	$k_{\text{0-eff}}(T,P,\underline{X})/k_0(T,\underline{X})$	$\langle\Delta E_d\rangle(T)$ †
Ar	12		5.04	0.78	
	15	4.93	4.93	0.76	162.85
	18		4.84	0.75	
	20		4.78	0.74	
	25		4.65	0.72	
	30		4.55	0.70	
N_2	12		6.99	0.76	
	15	6.82	6.82	0.74	186.15
	18		6.68	0.72	
	20		6.59	0.71	
	25		6.40	0.69	
	30		6.24	0.68	
H_2O/Ar ‡	12		117.01	0.73	
	15	113	112.82	0.71	862.33
	18		110.25	0.69	
	20		108.39	0.68	
	25		104.36	0.66	
	30		100.96	0.64	

$^{\top}$ from [12], units: 10^{-33}cm^{6}molecule^{-2}s^{-1};
$^{\perp}$ calculated using PAPR-MESS, units: 10^{-33}cm^{6}molecule^{-2}s^{-1};
‡ $X_{\text{H}_2\text{O}}/X_{\text{Ar}} = 10\%/90\%$;
† the listed exponential-down factors in the i/Ar mixture are for i, units: cm^{-1}.

Table S5: 2D/φ-ME Results at 296 K

M	P (Torr)	$k_{\text{i,0-eff, LMR-P,exp}}(T,P,\underline{X})^{\top}$	$k_{\text{i,0-eff}}(T,P)^{\perp}$	$k_{\text{0-eff}}(T,P)/k_0(T)$	$\langle\Delta E_d\rangle(T)$ †
Ar	25		2.21	1.00	
	50		2.21	1.00	
	75		2.20	1.00	
	100	2.2	2.20	1.00	52.05
	150		2.19	0.99	
	200		2.19	0.99	
N_2	25		4.30	1.00	
	50		4.30	0.99	
	75		4.29	0.99	
	100	4.3	4.29	0.99	102.02
	150		4.27	0.99	
	200		4.26	0.99	
H_2O	2.2		18.2		
	2.5		18.2		
	3		18.2		
	4		18.2		
	5	50	18.2		Strong-collision limit
	6		18.2		
	7		18.2		

$^{\top}$ from [10], units: 10^{-32}cm^{6}molecule^{-2}s^{-1};
$^{\perp}$ calculated using Variflex, units: 10^{-32}cm^{6}molecule^{-2}s^{-1};
† units: cm^{-1}.

Table S6: 2D/φ-ME Results at 1200 K

M	P (atm)	$k_{\text{i,0-eff, LMR-P,exp}}(T,P,\underline{X})^{\top}$	$k_{\text{i,0-eff}}(T,P)^{\perp}$	$k_{\text{0-eff}}(T,P)/k_0(T)$	$\langle\Delta E_d\rangle(T)$ †
Ar	12		4.97	0.95	
	15	4.93	4.93	0.94	204.71
	18		4.89	0.94	
	20		4.86	0.93	
	25		4.79	0.92	
	30		4.74	0.91	
N_2	12		6.89	0.95	
	15	6.82	6.82	0.94	240.69
	18		6.76	0.93	
	20		6.70	0.92	
	25		6.61	0.91	
	30		6.54	0.90	
H_2O	12		83.9		
	15	113	81.4		Strong-collision limit
	18		79.4		
	20		77.9		
	25		74.6		
	30		72.5		

$^{\top}$ from [12], units: 10^{-33}cm^{6}molecule^{-2}s^{-1};
$^{\perp}$ calculated using Variflex, units: 10^{-33}cm^{6}molecule^{-2}s^{-1};
† units: cm^{-1}.

Combining the results in Tables S3 and S4 for 1D-ME calculations and Tables S5 and S6 for 2D/φ-ME calculations, the temperature-dependent exponential-down factors for M = Ar, N_2, and H_2O are derived as presented in Table 5 in the main text using 1D-ME model and in Table S7 using 2D/φ-ME model. (Note that the calculated rate constants for H_2O from the 2D/φ-ME could not be made to reproduce the experimental values even in the strong-collision limit.)

Table S7: Temperature-dependent energy-transfer parameters from 2D/φ-ME model.

Ar	$\langle \Delta E_d \rangle_{\mathrm{Ar}} = 52.40 \times (T/298)^{0.978}$
N_2	$\langle \Delta E_d \rangle_{\mathrm{N_2}} = 102.45 \times (T/298)^{0.613}$
H_2O	—

S3 Comparisons of Calculations and Other Experiments

Results from 1D-ME and 2D/φ-ME calculations using the exponential-down factors from Table S7 and a priori 2D-ME calculations for Ar [8] with comparisons to reported experimental determinations [1, 2, 3, 4, 5, 6, 10, 12, 15] are shown in Figures S1–S4.

All three master equation models show reasonable agreement with experimental data (given the scatter in the experimental data) as shown in Figs. S1, S3, and S4. The a priori 2D-ME calculations, which are expected to be accurate within ∼20-30% [7, 8], unsurprisingly appear to yield the best agreement with the experimental data. The 1D-ME and 2D/φ-ME calculations, while different, show similar agreement with experimental data – at a level that still appears reasonable given the large scatter in most experimental datasets.

As shown in Fig. S2, the three master equation models yield similar results – with some slight differences on the order of ∼30% – which provides an indication of the sensitivity of the calculation to different treatments of angular momentum.

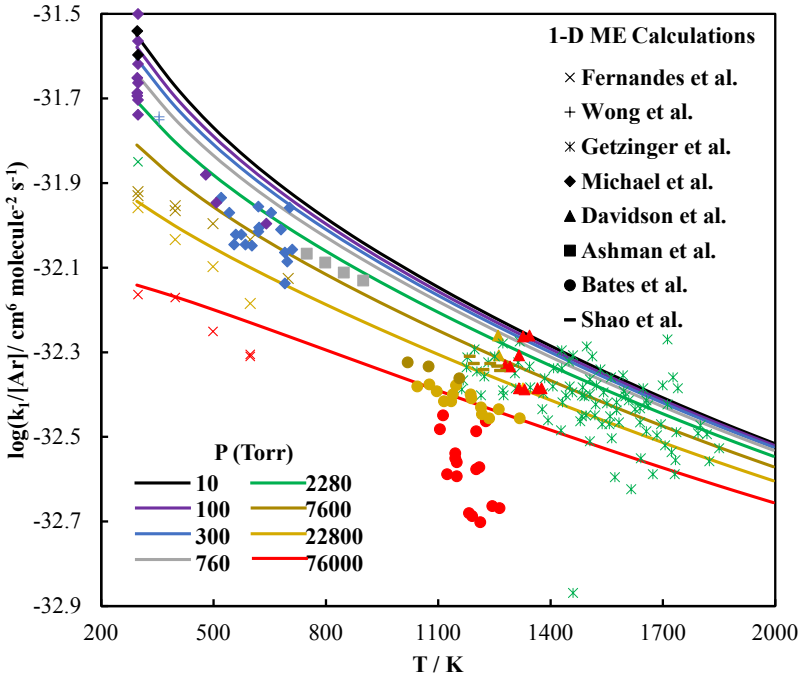
1-D ME Calculations
× Fernandes et al.
+ Wong et al.
⁎ Getzinger et al.
◆ Michael et al.
▲ Davidson et al.
■ Ashman et al.
● Bates et al.
– Shao et al.
P (Torr)
10
100
300
760
2280
7600
22800
76000
log(k1/[Ar]/ cm6 molecule-2 s-1)
T / K
-31.5
-31.7
-31.9
-32.1
-32.3
-32.5
-32.7
-32.9
200
500
800
1100
1400
1700
2000

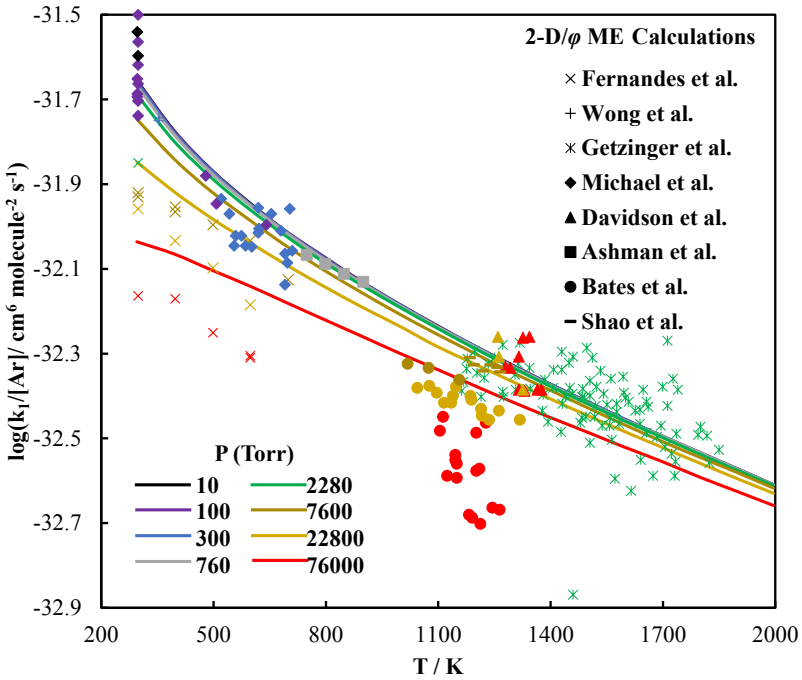
2-D/φ ME Calculations
× Fernandes et al.
+ Wong et al.
⁎ Getzinger et al.
◆ Michael et al.
▲ Davidson et al.
■ Ashman et al.
● Bates et al.
– Shao et al.
P (Torr)
10
100
300
760
2280
7600
22800
76000
log(k1/[Ar]/ cm6 molecule-2 s-1)
T / K
-31.5
-31.7
-31.9
-32.1
-32.3
-32.5
-32.7
-32.9
200
500
800
1100
1400
1700
2000

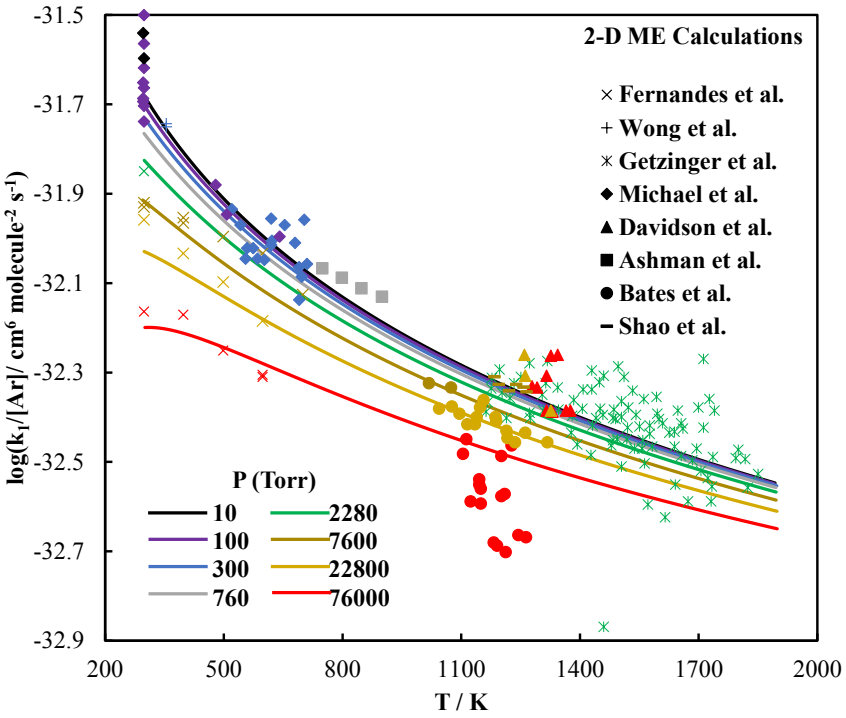

Figure S1: Ab initio master equation (ME) calculated temperature- and pressure-dependent rate constants for H + O_2 + Ar → HO_2 + Ar versus experimental determinations. The experimental data points [1, 2, 4, 5, 6, 10, 12, 15] are color coded according to the closest pressure from the theoretical calculations. Results are shown from a 1D-ME (E-resolved model) (top), a 2D/φ-ME (approximate E,J-resolved model) (middle), and an a priori 2D-ME (E,J-resolved model) [8] (bottom).

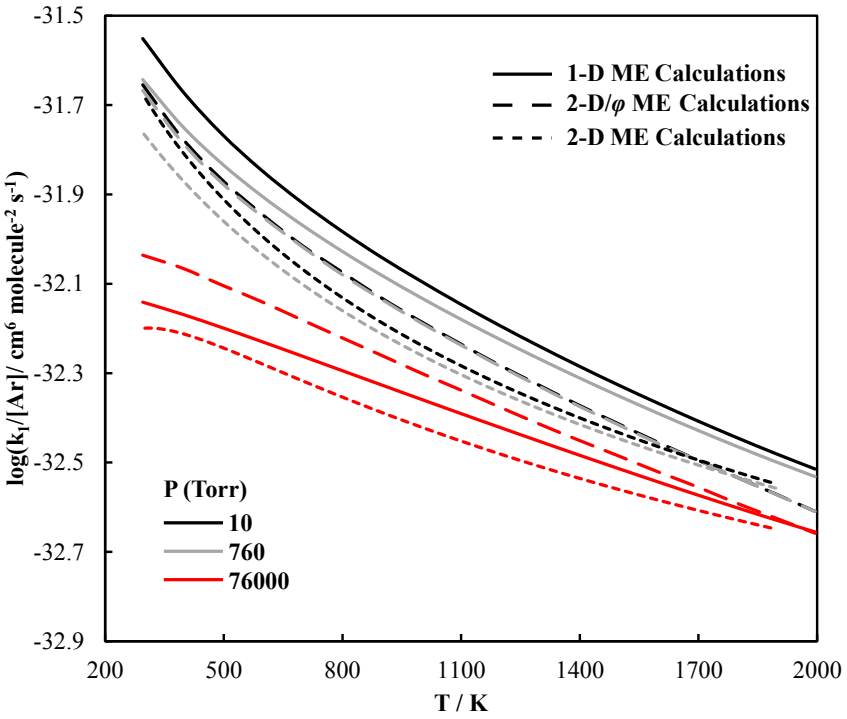

Figure S2: Ab initio master equation (ME) calculated temperature- and pressure-dependent rate constants for H + O_2 + Ar → HO_2 + Ar versus experimental determinations. Results are shown from a 1D-ME (E-resolved model) (solid lines), a 2D/φ-ME (approximate E,J-resolved model) (long dashed lines), and an a priori 2D-ME (E,J-resolved model) [8] (short dashed lines).

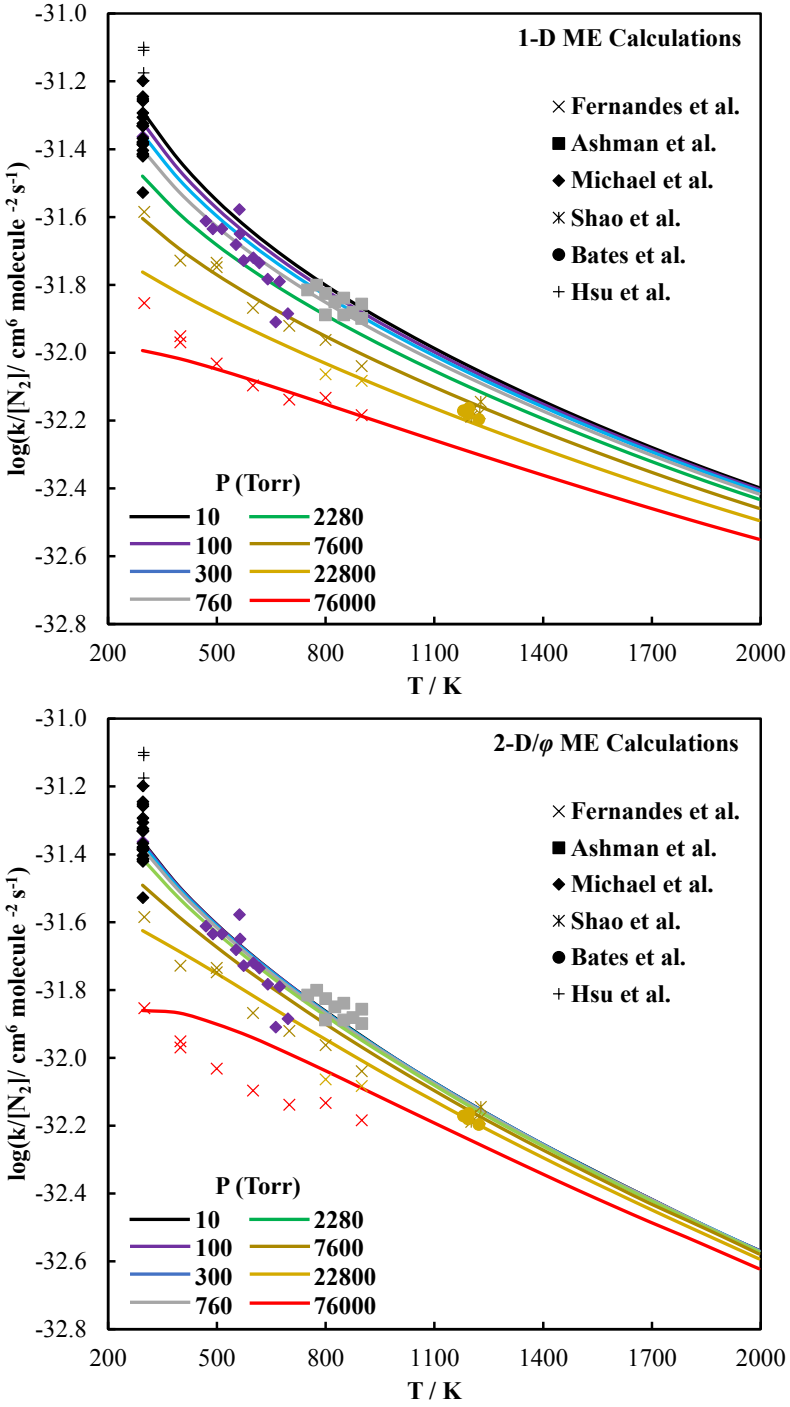

Figure S3: Ab initio master equation (ME) calculated temperature- and pressure-dependent rate constants for H + O_2 + N_2 → HO_2 + N_2 versus experimental determinations. The experimental data points [1, 2, 5, 10, 12] are color coded according to the closest pressure from the theoretical calculations. Results are shown from a 1D-ME (E-resolved model) (top) and a 2D/φ-ME (approximate E,J-resolved model) (bottom).

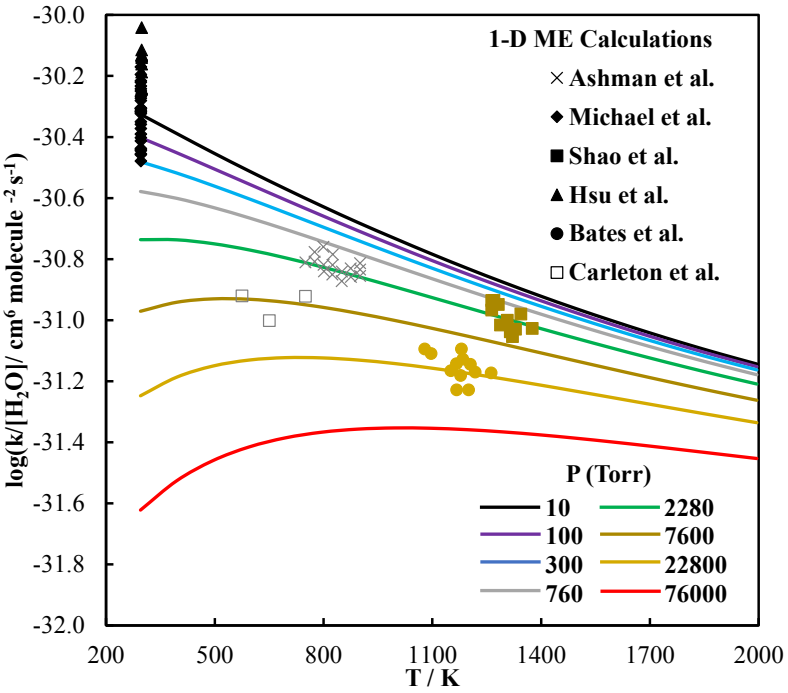

Figure S4: Ab initio master equation (ME) calculated temperature- and pressure-dependent rate constants for H + O_2 + H_2O → HO_2 + H_2O versus experimental determinations. The experimental data points [1, 2, 3, 10, 12] are color coded according to the closest pressure from the theoretical calculations. Results are shown from a 1D-ME (*E*-resolved model). Note that the calculated results plotted were obtained for pure H_2O, whereas the experimental determinations plotted were obtained in mixtures of various H_2O mole fractions using the linear mixture rule.

References

[1] P. J. Ashman and B. S. Haynes. Rate coefficient of H+O_2+M→HO_2+M (M=H_2O, N_2, Ar, CO_2). *Sym. (Int.) Combust.*, 27(1):185 – 191, 1998.

[2] R. W. Bates, D. M. Golden, R. K. Hanson, and C. T. Bowman. Experimental study and modeling of the reaction H+O_2+M → HO_2+M (M = Ar, N_2, H_2O) at elevated pressures and temperatures between 1050 and 1250 K. *Phys. Chem. Chem. Phys.*, 3(12):2337–2342, 2001.

[3] K. L. Carleton, W. J. Kessler, and W. J. Marinelli. Hydrogen atom + oxygen + M (= N_2, H_2O, Ar) three-body rate coefficients at 298-750 K. *J. Phys. Chem.*, 97(24):6412–6417, 1993.

[4] D. Davidson, E. Petersen, M. Röhrig, R. Hanson, and C. Bowman. Measurement of the rate coefficient of H + O_2 + M → HO_2 + M for M=Ar and N_2 at high pressures. *Sym. (Int.) Combust.*, 26(1):481 – 488, 1996.

[5] R. X. Fernandes, K. Luther, J. Troe, and V. G. Ushakov. Experimental and modelling study of the recombination reaction H + O_2 (+M) → HO_2 (+M) between 300 and 900 K, 1.5 and 950 bar, and in the bath gases M = He, Ar, and N_2. *Phys. Chem. Chem. Phys.*, 10:4313–4321, 2008.

[6] R. Getzinger and L. Blair. Recombination in the hydrogen-oxygen reaction: A shock tube study with nitrogen and water vapour as third bodies. *Combust. Flame*, 13(3):271 – 284, 1969.

[7] A. W. Jasper, K. M. Pelzer, J. A. Miller, E. Kamarchik, L. B. Harding, and S. J. Klippenstein. Predictive a priori pressure-dependent kinetics. *Science*, 346(6214):1212–1215, 2014.

[8] S. J. Klippenstein. From theoretical reaction dynamics to chemical modeling of combustion. *Proc. Combust. Inst.*, 36(1):77–111, 2017.

[9] A. I. Maergoiz, E. E. Nikitin, J. Troe, and V. G. Ushakov. Classical trajectory and adiabatic channel study of the transition from adiabatic to sudden capture dynamics. III. Dipole–dipole capture. *J. Chem. Phys.*, 105(15):6277–6284, 1996.

[10] J. V. Michael, M.-C. Su, J. W. Sutherland, J. J. Carroll, and A. F. Wagner. Rate constants for H + O_2 + M → HO_2 + M in seven bath gases. *J. Phys. Chem. A*, 106(21):5297–5313, 2002.

[11] P. Paul and J. Warnatz. A re-evaluation of the means used to calculate transport properties of reacting flows. *Sym. (Int.) Combust.*, 27(1):495 – 504, 1998.

[12] J. Shao, R. Choudhary, A. Susa, D. F. Davidson, and R. K. Hanson. Shock tube study of the rate constants for H + O_2 + M → HO_2 + M (M = Ar, H_2O, CO_2, N_2) at elevated pressures. *Proc. Combust. Inst.*, 37(1):145 – 152, 2019.

[13] R. D. Johnson III. NIST Computational Chemistry Comparison and Benchmark Database. *NIST Standard Reference Database Number 101*, (Release 19), April 2018.

[14] J. Troe and V. Ushakov. personal communication.

[15] W. Wong and D. Davis. A flash photolysis-resonance fluorescence study of the reaction of atomic hydrogen with molecular oxygen H + O_2 + M → HO_2 + M. *Int. J. Chem. Kinet.*, 6(3):401–416, 1974.